Earth and Planetary Science Letters 383 (2013) 68–81

Contents lists available at ScienceDirect

Earth and Planetary Science Letters

www.elsevier.com/locate/epsl

A simple model for chalcophile element partitioning between sulphide and silicate liquids with geochemical applications

Ekaterina S. Kiseeva *, Bernard J. Wood

Department of Earth Sciences, University of Oxford, Oxford OX1 3AN, UK

ARTICLE INFO

Article history:
Received 16 March 2013
Received in revised form 16 September 2013
Accepted 20 September 2013
Available online 16 October 2013
Editor: T. Elliot

Keywords:
sulphide–silicate partitioning
chalcophile elements
high pressure experiments
trace elements
lead paradoxes
depleted mantle

ABSTRACT

We have determined the partitioning of the elements Cu, In, Tl, Pb, Ag, Mn, Zn, Cr, Co, Ni, Sb and Cd between FeS-rich sulphide liquids and anhydrous basaltic melts at high pressures and temperatures. The sulphide liquids were found to have oxygen contents which are linearly related to the FeO contents of the silicate melts. We also found simple relationships between the FeO contents of the silicate melts and the sulphide–silicate partition coefficients $D_M^{sulph/sil}$ for the individual trace elements. These relationships can be generally represented as follows:

$$\log D_M^{sulph/sil} \approx A + \frac{n}{2}\log[FeO]$$

where A is a constant related to the free energy of Fe–M exchange, n is a constant related to the valence of the element and [FeO] is the FeO content of the silicate melt in mole fraction or weight %. This simple relationship effectively removes the need to define the fugacity ratio f_{O_2}/f_{S_2} when considering partitioning and hence greatly simplifies application of partitioning data to natural systems. In theory n should approximate −1 for 1+ ions, −2 for 2+ ions and so on. Regressed values of n are generally close to those expected, although deviations occur for some elements. The deviations can be understood in terms of the relative chalcophile and lithophile characteristics of the element of concern.

For cases in which the sulphide is an FeS–NiS–Cu_2S liquid we obtain excellent agreement with results for pure FeS by correcting the FeO content of the silicate melt as follows:

$$[FeO]_{corrected} = \frac{[FeO]_{silicate}}{[Fe/(Fe+Ni+Cu)]_{sulphide}}$$

We tested our model on data from the literature in which sulphide–silicate partition coefficients for Cu, Co, Ni and Mn were determined. Literature data for these elements follow the predicted linear dependence of $\log D_M^{sulph/sil}$ on log[wt% FeO]. Furthermore, differences between the absolute values of $D_M^{sulph/sil}$ obtained by us and those in the literature are quantifiable in terms of temperature and matrix effects such as the Ni/Fe ratio of the sulphide.

We used our results for Pb partitioning to calculate Ce/Pb and Nd/Pb ratios of basalts generated by partial melting of the mantle followed by fractional crystallization. Calculated Nd/Pb is essentially constant over wide ranges of partial melting and fractional crystallization with a value of ~18.6 if we assume that depleted mantle contains 65 ppb of Pb. Calculated Ce/Pb varies slightly during batch partial melting from 21 to 29 with the canonical value of 25 being achieved at ~10% partial melting. These trends are in excellent agreement with measurements of oceanic basalt glasses.

Finally, we used our partitioning relationships to calculate the concentrations of a number of the incompatible chalcophile trace elements in depleted mantle. These are as follows: 32 ppm Cu, 65 ppb Pb, 7.6 ppb Ag, 12 ppb In, 23 ppb Cd, 1.7 ppb Sb and 1.3 ppb Tl.

1. Introduction

Despite the concentration of sulphur in the silicate Earth being only about 250 ppm (McDonough and Sun, 1995), sulphur and sulphides are known to be very important geochemical agents in all petrogenetic environments. The presence of immiscible sul-

* Corresponding author.
E-mail addresses: kate.kiseeva@earth.ox.ac.uk (E.S. Kiseeva), berniew@earth.ox.ac.uk (B.J. Wood).

0012-821X/$ – see front matter
http://dx.doi.org/10.1016/j.epsl.2013.09.034

phide globules in basaltic magmas indicates, for example, sulphide saturation at the time of eruption (Mathez, 1976; Wallace and Carmichael, 1992) and the decreasing solubility of S in silicate melts with increasing pressure (Holzheid and Grove, 2002) implies that MORB are generally at sulphide saturation throughout their path of ascent to the surface. The ability of sulphides to concentrate chalcophile elements is economically important in the context, for example, of high temperature copper porphyry deposits and low temperature lead–zinc deposits. Many other chalcophile elements (Cd, In, for example) are economically important, which makes the interpretation and understanding of their geochemical behavior of considerable value. There are, however, few data on the partitioning of these elements into sulphides under high temperature petrogenetic conditions.

In addition to economic importance, sulphide and chalcophile elements have played important roles in the accretion and differentiation of the Earth. The relatively low abundance of S in the silicate Earth is probably due to its strong partitioning into the core during accretion (Dreibus and Palme, 1996) plausibly as a late-added sulphide matte (O'Neill, 1991; Wood and Halliday, 2005). The effects of such a matte would be to remove large fractions of chalcophile elements such as the platinum group elements (PGE) Pb, Cu and Ag to the Earth's core with corresponding increase in ratios such as U/Pb in the silicate Earth (Hart and Gaetani, 2006; Wood and Halliday, 2005). Wood and Halliday (2005) suggested that Pb partitioning into such a matte would be so strong that removal of $< 1\%$ by mass would be sufficient to shift μ ($^{238}U/^{204}Pb$) of the silicate Earth from the CI chondrite value (0.7) to the current value of ~ 9. Hart and Gaetani (2006) suggested that continuing dissolution of such a mantle sulphide into the core could be responsible for the "lead paradox", the observation that silicate Earth lies to the right of the "geochron" on a $^{207}Pb/^{204}Pb$ vs. $^{206}Pb/^{204}Pb$ diagram. The latter indicates that U/Pb fractionation occurred on Earth considerably later than the time of core formation given by Earth's ^{182}W anomaly (relative to chondrites) either in a single late core addition event (Wood and Halliday 2005, 2010; Rudge et al., 2010) or through progressive Pb extraction through geologic time (Hart and Gaetani, 2006). In either case, accurate modeling of the effects of sulphide extraction has been hampered by insufficient data on $D_{Pb}^{sulph/sil}$, the partition coefficient for Pb between sulphide and silicate melt. The importance of sulphide in controlling the behavior of Pb in the mantle is emphasized by data showing that silicates from a selectively leached peridotite contained only about 10% of the total expected amount of Pb, with the inference that the remainder resides in sulphide (Meijer et al., 1990). This conclusion was confirmed by recent studies showing the presence of significant amounts of unradiogenic lead, with ^{207}Pb–^{206}Pb age of about 2 Gyr in sulphides from abyssal peridotites (Burton et al., 2012; Warren and Shirey, 2012). The latter lie well to the left of the geochron and could provide a major part of the reservoir complementing the Pb–isotope compositions of crust and MORB source regions.

Since the Ce/Pb and Nd/Pb ratios of N-MORB are essentially constant at ~ 25 and ~ 20 respectively, it is generally assumed that lead behaves in a similar manner to these rare earths during partial melting and fractional crystallization (Hart and Gaetani, 2006; Hofmann et al., 1986). However, almost all measurements of silicate crystal-melt partition coefficients show that Pb is much more incompatible than Ce and Nd (Hart and Gaetani, 2006), which means that partitioning of Pb into sulphide exerts the principal control on behavior of this element during melting and differentiation. As noted above, however, lack of reliable sulphide/silicate partition coefficients hinders understanding of the relationship between Pb, Nd and Ce. A summary of available data on $D_{Pb}^{sulph/sil}$ demonstrates, for example, a measured range from 1.3 to 40 (Hart and Gaetani, 2006) with a possible dependence on the oxygen content of the sulphide melt.

Lee et al. (2012) argue for an important role of sulphide precipitation in controlling the behavior of Cu during generation and evolution of island arc basalts. Their summary of literature data indicates that Cu is strongly incompatible in most silicate phases and that with $D_{Cu}^{sulph/sil}$ in the range 600–1200 the small amounts of sulphide present in the arc mantle control the Cu contents of magmas. Furthermore, they suggest that the low Cu concentrations in primitive arc basalts imply oxygen fugacities of $\sim$ FMQ (similar to MORB) and that some differentiated magmas reach about FMQ + 1.3 before precipitating sulphide (Lee et al., 2012). In contrast to these conclusions, a recent experimental study of silicate crystal-melt partitioning of Cu (Fellows and Canil, 2012) indicates greater compatibility of this element in silicate and a conclusion that sulphide is much less important in controlling Cu concentrations in magmas than was supposed by Lee et al. (2012). More accurate measurements of $D_{Cu}^{sulph/sil}$ for basaltic magmas would help resolve this issue.

To date, a large proportion of sulphide–silicate partitioning studies have concerned themselves with the platinum group elements (Bockrath et al., 2004; Crocket et al., 1997; Fleet et al., 1996, 1991) and relatively few with the chalcophile elements such as Cu, Co, Pb, Sb, Bi and Ag discussed above (Gaetani and Grove, 1997; Li and Audétat, 2012; Wood et al., 2008). In order to address their geochemical behavior, Li and Audétat (2012) recently made a comprehensive study of partitioning of a large number of elements (V, Mn, Co, Ni, Cu, Zn, As, Mo, Ag, Sn, Sb, W, Au, Pb, Bi) between solid and liquid sulphides and hydrous basanite melt at high pressure. These authors followed Gaetani and Grove (1997) in recognizing the importance of oxygen fugacity in determining sulphide–silicate partitioning. This can be appreciated from the equilibrium of an element such as Co between silicate and sulphide phases:

$$\underset{\text{silicate}}{\text{CoO}} + 0.5S_2 = \underset{\text{sulphide}}{\text{CoS}} + 0.5O_2 \tag{1}$$

The equilibrium constant for reaction (1) can be written as:

$$K_1 = \frac{a_{CoS}^{sulph} \cdot f_{O_2}^{0.5}}{a_{CoO}^{sil} \cdot f_{S_2}^{0.5}} \tag{2}$$

where K_1 is the equilibrium constant and a_i and f_i are activity and fugacity of i respectively. In general, the activity of a component is closely related to its concentration in the phase of interest, so, to a good approximation we can simplify (2) as follows:

$$\frac{a_{CoS}^{sulph}}{a_{CoO}^{sil}} \approx \frac{[Co]^{sulph}}{[Co]^{sil}} = D_{Co}^{sulph/sil} = K_1' \cdot \frac{f_{S_2}^{0.5}}{f_{O_2}^{0.5}} \tag{3}$$

where K_1' is a modified equilibrium constant in terms of concentration $[Co]^{sulph}$ and $[Co]^{sil}$. Thus, the partition coefficients D_i must depend on the ratio of sulphur fugacity to oxygen fugacity. To account for these dependences Li and Audétat attempted to control oxygen fugacity in piston–cylinder experiments using external buffers such as Ni–NiO with a hydrous fluid. They then calculated sulphur fugacity after the experiment from the ratio FeO^{sil}/FeS^{sulph}. The principal difficulties and uncertainties in this approach are firstly that diffusion of hydrogen through the inner metal capsule caused reaction and loss of sulphide as H_2S and FeO in experiments of more than 2 h duration. Secondly, changing water and FeO contents of the silicate with time makes it difficult to ensure that equilibrium is approached. Since many of the elements of interest are volatile, the alternative approach of performing the experiments at 1 bar with controlled f_{O_2} and f_{S_2} may not be productive. However, in sulphide-saturated experiments at

Table 1
Experimental results.

Run No.	Starting composition	Duration (h)	Capsule	Olivine layer
KK3-1	MORB + FeS	3	Graphite	No
KK3-2	MORB + FeS	4	Graphite	Yes-single
KK4-1	MORB + FeS + 0.5% NiS	2	Graphite	Yes-single
KK4-3	MORB + FeS + 0.5% NiS	19.5	Graphite	Yes-single
KK4-5	MORB + FeS + 0.5% NiS	5	Graphite	Yes-single
KK5-1	MORB + FeS + 10% NiS	2	Graphite	Yes-single
KK5-2	MORB + FeS + 10% NiS	5	Graphite	Yes-single
KK6-1	MORB + FeS + 5% NiS	5	Graphite	Yes-double
KK6-3	MORB + FeS + 5% NiS	1.5	Graphite	Yes-double
KK7-1	MORB + FeS + 2.5% NiS	2	Graphite	Yes-single
KK7-2	MORB + FeS + 2.5% NiS	5	Graphite	Yes-single
KK8-1	MORB + FeS + 17.5% NiS	2.5	Graphite	Yes-single
KK8-2	MORB + FeS + 17.5% NiS	5.3	Graphite	Yes-single
KK12-1	MORB + FeS + 0.5% NiS + 33% FeO	2	Graphite	No
KK15-1	MORB + FeS + 0.5% NiS + 20% FeO	2	Pt–Graphite	No
KK15-2	MORB + FeS + 0.5% NiS + 20% FeO	1	Graphite	No
KK15-4	MORB + FeS + 0.5% NiS + 20% FeO	7	Graphite	No
KK15-5	MORB + FeS + 0.5% NiS + 20% FeO	0.5	Graphite	No
KK16-1	CMAS + FeS + 0.5% NiS	2	Graphite	No
KK16-2	CMAS + FeS + 0.5% NiS	3.5	Graphite	No

known FeO activity in the silicate melt, the ratio f_{O_2}/f_{S_2} is fixed. This means that we can use closed-system experiments at high pressure and measure the exchange partition coefficient involving Fe and the element of interest without making explicit provisions for, or calculations of, the ratio f_{O_2}/f_{S_2}. Thus, for Co, for example, we consider the equilibrium:

$$\underset{\text{silicate}}{\text{CoO}} + \underset{\text{sulphide}}{\text{FeS}} = \underset{\text{silicate}}{\text{FeO}} + \underset{\text{sulphide}}{\text{CoS}} \quad (4)$$

At saturation of the silicate melt with sulphide we can formulate the Co partition coefficient $D_{\text{Co}}^{sulph/sil}$ in terms of a modified equilibrium constant K_4' and the activities of iron species which are much easier to measure and control than the fugacities of the gaseous species:

$$D_{\text{Co}}^{sulph/sil} = K_4' \frac{a_{\text{FeS}}^{sulph}}{a_{\text{FeO}}^{sil}} \quad (5)$$

Our objective was to extend the exchange approach of Eq. (4) to measure and parameterize liquid sulphide–liquid silicate partition coefficients for the chalcophile elements Cu, In, Tl, Pb, Ag, Zn, Cr, Co, Sb, Cd, Ni and Mn at high pressure and temperature. As will be shown, the method enables a simple chemical parameterization of the partition coefficients and provides for extrapolation using just the compositions of the coexisting silicate and sulphide phases.

2. Experimental and analytical procedures

2.1. Experimental methods

Starting materials consisted of mixtures of ~ 50% (Fe, Ni)S and ~ 50% synthetic silicate, by weight. The silicate constituent was either a MORB (Falloon and Green, 1987) or a composition close to the 1.5 GPa eutectic composition in the system anorthite–diopside–forsterite ($An_{50}Di_{28}Fo_{22}$) (Presnall et al., 1978) (Table 1). The silicates were prepared from analytical grade oxides (SiO_2, TiO_2, Al_2O_3, MgO, Fe_2O_3, MnO_2, P_2O_5) and carbonates (Na_2CO_3, K_2CO_3, $CaCO_3$). Prior to adding Fe_2O_3, the mixtures were decarbonated at 950 °C for 2 h. After Fe_2O_3 was added, mixtures were reground, pelletised and reduced at 1-atmosphere for 2 h at 1000 °C and oxygen fugacity of IW + 2. Additional Fe (as $Fe_{0.95}O$) was added to some experiments in order to increase FeO activity. Olivine (as synthetic Fo_{90}) was added as a layer placed in the bottom of the charge in some experiments to ensure olivine saturation appropriate for MORB generation. All experiments were doped with a previously prepared trace element mixture containing Cu, In, Tl, Pb, Ag, Zn, Cr, V, Co, Sb and Cd as oxides. With the exception of Cu_2O, the oxides were at concentrations of about 1000 ppm in the metal–silicate starting mixtures. The proportion of Cu_2O was twice that of the other oxides to enable use of Cu as a check on analysis of the sulphides by Laser Ablation ICP-MS (LA-ICPMS). Various amounts of Ni (as NiS) were added to the sulphide component. The starting materials were ground under acetone to ensure a homogeneous mix before being dried prior to the experiment.

Starting mixtures were loaded into 3 mm O.D., 1 mm I.D. graphite capsules, with one experiment (KK15-1) using an additional outer Pt capsule. This approach was used to ensure that the experimental oxygen fugacity was close to the C–CO_2 buffer.

Experiments were performed in an end-loaded Boyd–England-type piston–cylinder apparatus at the University of Oxford. More complete experimental and analytical details are provided in Supplementary Information.

2.2. Approach to equilibrium and mass balance

In order to determine the experiment duration required for attainment of chemical equilibrium between the sulphide liquid and silicate melt, a set of isothermal time series experiments was conducted in olivine-free starting materials (Fig. 1a). In Fig. 1a we plot data for 4 elements which have similar partition coefficients and which can be readily compared on a linear graph of $D_{\text{M}}^{sulph/sil}$ vs. experiment duration. As can be seen, experiment durations of 0.5 to 7 h generally produce results within 1 standard deviation of one another so that 30 min should be adequate for an approach to equilibrium. This conclusion is in agreement with metal-silicate partitioning experiments on charges of similar volume (Tuff et al., 2011). We also found that when more than one sulphide blob was present they were compositionally indistinguishable from one another. Despite the apparent rapidity of approach to equilibrium, however, we extended our experiment times to between 2 and 5 h to provide additional assurance of equilibrium partitioning.

Experiment durations longer than 7 h were not normally used because of the reported loss of Cu (Fellows and Canil, 2012) and Ni (A. Matzen, personal communication), from graphite capsules in long duration experiments. We checked for loss by mass-balancing our analyses to the known amounts of trace element added to the starting compositions for those experiments where we had

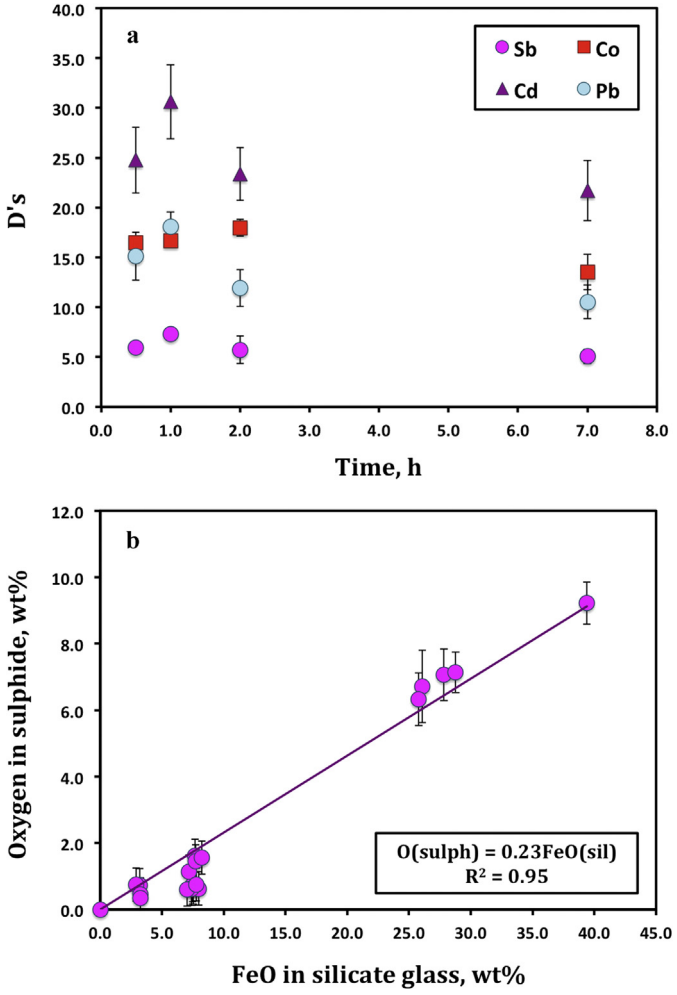

Fig. 1. Experimental results. (a) Time-series experiments conducted to assess the experiment duration required in order to approach equilibrium, illustrated here as $D^{sulphide/silicate}$ values plotted against run time. Error bars are propagated from one standard deviation of repeat analyses of sulphide and silicate in each run. (b) Oxygen content of the sulphide as a function of the FeO content of the silicate glass. Errors assumed to be ±0.5 wt% O or one standard deviation, whichever is higher.

only silicate melt and sulphide liquid present (i.e. no olivine). We found that very little Cu (generally < 10% relative) is lost from our capsule configuration at run durations up to 7 h, but that large amounts of Ni (between 25 and 60% of the amount present) is lost. The observation of extensive Ni loss concurs with unpublished results of A. Matzen (personal communication), who has been studying Ni partitioning between olivine and silicate melt. Ni loss may be due to the formation of gaseous $Ni(CO)_4$ which, although unstable above 180 °C at low pressure, should be stabilized by high pressure because of the large volume change of the breakdown reaction. We found no significant loss of any of the other elements and recorded slight gains in Mn and Cd. We believe that the latter are due to contamination of major Fe_2O_3 and $CaCO_3$ starting compounds by small amounts of Mn and Cd respectively.

3. Results

Major element compositions of experimentally-produced silicate and sulphide phases are presented in Tables 2 and 3. All the trace elements added to the starting materials were above detection limits in both sulphide and silicate phases in all experiments and are apparently homogeneously distributed in both phases. The olivine crystals, where present, were very small (typically, about 10–20 μm) and usually had small amounts of melt residing along the grain boundaries, which hindered direct LA-ICPMS analysis.

3.1. Oxygen in the sulphide

Equilibrium between sulphide (in the system Fe–Ni–S–O) and silicate means that the FeO activity must be the same in both phases:

$$K_{ox} = \frac{a^{sulph}_{FeO}}{a^{sil}_{FeO}} = 1 = \frac{X^{sulph}_{FeO}\gamma^{sulph}_{FeO}}{X^{sil}_{FeO}\gamma^{sil}_{FeO}} \quad (6)$$

In Eq. (6), a_{FeO} refers to activity and X_{FeO} and γ_{FeO} to mole fraction of FeO and its activity coefficient respectively. Given Eq. (6), it is clear that the concentration of oxygen, as FeO, in the sulphide should depend on the FeO content of the silicate melt. Fig. 1b shows that the correlation between the two is excellent.

Noting that, if the FeO concentration in the silicate is zero the FeO content of the sulphide and hence its oxygen content must be zero, we regressed the O content (wt%) of sulphide vs. FeO content (wt%) of the silicate with a forced intercept of zero. As can be seen in Fig. 1b, the result is a slope of 0.23 ± 0.01 with an R^2 of 0.95. This compares with a theoretical slope, based on atomic weights, of 0.223.

The close agreement between "fitted" and "ideal" slopes (Fig. 1b) means that the ratio of the FeO activity coefficient in the sulphide to that in the silicate must be ~ 1. Since activity coefficients of FeO in basalt-like liquids are close to 1.0 (O'Neill and Eggins, 2002), this requires that FeO–FeS liquids are also close to ideal. Measurements at 1473 K (Nagamori and Yazawa, 2001) bear out this latter conclusion, activity of FeO being close to mole fraction for the composition range 3–10% oxygen.

Addition of significant amounts of Ni or Cu to the sulphide may decrease O solubility at fixed f_{O_2}/f_{S_2} (Fonseca et al., 2008), but not all authors are in agreement with this suggestion (Yoshikigravelsins and Toguri, 1993) and we see no evidence for it in our limited dataset.

3.2. Partition coefficient values as a function of FeO content of the silicate melt

As discussed in the introduction, we have performed closed-system experiments at sulphide saturation in order to determine trace element partitioning between sulphide and silicate liquids. Since the experiments were performed in carbon capsules, we consider that the oxygen fugacity was generally close to the C–CO_2 buffer 1 log f_{O_2} unit below FMQ. We did not, however, have any direct control over the f_{O_2}/f_{S_2} ratio, and cannot, therefore, take explicit account of the effect of oxygen fugacity on partition coefficients. We therefore used the exchange coefficient approach as exemplified by Eqs. (4) and (5) describing Co partitioning.

If we generalize the approach outlined for cobalt to an element M of known oxidation state n then, provided n is the same in both silicate and sulphide phases, we can consider the equilibrium for exchange of M and Fe between coexisting silicate and sulphide as follows:

$$\underset{\text{silicate}}{MO_{n/2}} + (n/2)\underset{\text{sulphide}}{FeS} = \underset{\text{sulphide}}{MS_{n/2}} + (n/2)\underset{\text{silicate}}{FeO} \quad (7)$$

For reaction (7) the equilibrium constant in terms of activities and mole fractions can be expressed as follows:

$$K_7 = \frac{X^{sulph}_{MS_{n/2}}\gamma^{sulph}_{MS_{n/2}}(X^{sil}_{FeO}\gamma^{sil}_{FeO})^{n/2}}{X^{sil}_{MO_{n/2}}\gamma^{sil}_{MO_{n/2}}(a^{sulph}_{FeS})^{n/2}} \quad (8)$$

Table 2
Major element compositions of the silicate glass.

Run No.	KK3-1		KK3-2		KK4-1		KK4-3		KK5-1	
n	12	σ	23	σ	12	σ	20	σ	22	σ
SiO_2	50.55	0.51	48.23	0.31	50.30	0.67	48.27	0.13	49.34	0.55
TiO_2	0.82	0.02	0.70	0.02	0.73	0.03	0.73	0.01	0.72	0.09
Al_2O_3	15.38	0.15	12.75	0.15	13.38	0.24	13.82	0.09	13.52	0.18
FeO	7.50	0.09	7.98	0.12	7.42	0.13	7.40	0.09	7.15	0.17
MgO	10.44	0.13	16.29	0.15	15.56	0.19	14.25	0.07	15.72	0.21
CaO	12.62	0.08	10.48	0.12	10.74	0.07	11.17	0.07	10.18	0.11
Na_2O	1.37	0.29	1.76	0.04	1.32	0.24	2.40	0.03	1.22	0.23
K_2O	n.m.		n.m.		n.m.		n.m.		n.m.	
P_2O_5	n.m.		n.m.		n.m.		n.m.		n.m.	
SO_2	0.35	0.02	n.m.		0.39	0.02	n.m.	0.45	0.12	
Total	99.17		98.19		99.97		98.03		98.42	

Run No.	KK5-2		KK6-1		KK6-3		KK7-1		KK7-2	
n	12	σ	25	σ	25	σ	12	σ	27	σ
SiO_2	46.52	0.10	47.94	0.11	48.85	0.29	48.05	0.15	46.68	0.19
TiO_2	0.61	0.02	0.70	0.01	0.68	0.01	0.68	0.03	0.64	0.02
Al_2O_3	15.30	0.04	13.40	0.06	12.88	0.12	12.96	0.18	12.18	0.08
FeO	6.67	0.08	7.69	0.06	7.73	0.06	8.08	0.10	7.78	0.06
MgO	12.79	0.05	15.71	0.07	17.15	0.22	15.89	0.24	17.22	0.16
CaO	12.18	0.08	10.78	0.03	10.25	0.05	10.60	0.09	11.82	0.13
Na_2O	2.06	0.03	1.61	0.02	1.65	0.06	1.67	0.04	1.66	0.04
K_2O	0.17	0.01	n.m.		n.m.		0.14	0.00	n.m.	
P_2O_5	0.13	0.01	n.m.		n.m.		0.12	0.01	n.m.	
SO_2	0.44	0.02	n.m.		n.m.		0.45	0.02	n.m.	
Total	96.98		97.82		99.19		98.72		97.99	

Run No.	KK8-1		KK8-2		KK12-1		KK15-1		KK15-2	
n	23	σ	24	σ	16	σ	28	σ	18	σ
SiO_2	48.75	0.34	50.70	0.20	30.99	0.33	38.01	0.13	35.68	0.21
TiO_2	0.60	0.02	0.66	0.02	0.47	0.02	0.61	0.02	0.55	0.01
Al_2O_3	10.03	0.08	12.54	0.09	9.69	0.13	11.99	0.08	10.64	0.07
FeO	3.40	0.49	3.27	0.14	40.06	0.60	26.07	0.21	25.79	0.31
MgO	22.94	0.23	19.75	0.16	6.87	0.10	7.97	0.04	8.36	0.06
CaO	11.27	0.08	10.00	0.04	7.81	0.11	9.48	0.05	12.61	0.14
Na_2O	0.82	0.04	0.81	0.04	1.38	0.04	1.42	0.02	1.33	0.02
K_2O	n.m.		n.m.		0.10	0.01	n.m.		0.12	0.01
P_2O_5	n.m.		n.m.		0.10	0.01	n.m.		0.16	0.02
SO_2	0.55	0.41	0.42	0.11	2.68	0.55	1.36	0.08	1.30	0.30
Total	98.37		98.16		100.27		97.03		96.67	

Run No.	KK15-4		KK15-5		KK16-1		KK16-2	
n	49	σ	42	σ	41	σ	32	σ
SiO_2	37.48	0.20	37.19	0.17	44.75	0.13	45.10	0.16
TiO_2	0.58	0.02	0.58	0.02				
Al_2O_3	11.36	0.11	11.25	0.12	17.36	0.08	17.30	0.09
FeO	27.80	0.21	28.78	0.25	3.18	0.06	2.90	0.05
MgO	8.12	0.05	8.04	0.11	16.99	0.09	16.25	0.05
CaO	9.68	0.08	9.27	0.08	16.71	0.08	16.95	0.06
Na_2O	1.45	0.02	1.43	0.03				
K_2O	0.12	0.01	0.12	0.01				
P_2O_5	0.13	0.01	0.10	0.01				
SO_2	1.33	0.08	1.34	0.12	0.58	0.05	0.56	0.03
Total	98.20		98.24		99.57		99.06	

n.m. – not measured. *n* refers to number of analyses.

If we perform experiments in which the sulphide is close to FeS in composition (with small amounts of trace elements and oxygen dissolved), then a_{FeS}^{sulph} is close to 1.0. Similarly for trace M in sulphide and silicate we can make the initial assumption that the ratio of activity coefficients $\frac{\gamma_{MS_{n/2}}^{sulph}}{\gamma_{MO_{n/2}}^{sil}}$ is essentially constant during a series of isothermal/isobaric experiments when major element compositions of phases vary little. In justification of this assumption, our assessment of activity coefficients of NiO (γ_{NiO}) in silicate melts (Wood and Wade, 2013) leads to a spread in $\frac{\gamma_{MS_{n/2}}^{sulph}}{\gamma_{MO_{n/2}}^{sil}}$ of only ±0.1 log units when applied to the total range of sulphide and silicate compositions used in this study. Converting from mole fractions of M species to $D_M^{sulph/sil}$ as in Eq. (3) we obtain:

$$D_M^{sulph/sil} \cong K_7'' \frac{1}{(X_{FeO}^{sil} \cdot \gamma_{FeO}^{sil})^{n/2}} \quad (9)$$

In Eq. (9) K_7'' is a modified equilibrium constant which incorporates the additional activity coefficients and the factor for conversion of mole fractions to weight fractions. Noting that γ_{FeO}^{sil} is a weak function of composition (O'Neill and Eggins, 2002), we anticipate a simple relationship between $D_M^{sulph/sil}$ and the amount of FeO (mole fraction or wt%) in the melt:

$$\log D_M^{sulph/sil} \approx A + \frac{n}{2} \log[FeO] \quad (10)$$

Table 3
Major element compositions of the sulphide.

Run No.	KK3-1		KK3-2		KK4-1		KK4-3		KK5-1	
n	21	σ	32	σ	35	σ	20	σ	29	σ
O	0.67	0.19	0.63	0.26	0.73	0.23	0.62	0.11	1.13	0.54
S	36.77	0.48	36.09	0.25	36.98	0.56	36.60	0.25	36.32	0.61
Fe	61.34	0.59	62.10	0.29	60.96	0.39	61.74	0.47	54.70	0.47
Ni	–	–	–	–	0.35	0.03	0.33	0.02	6.54	0.12
Cu	0.28	0.01	0.29	0.04	0.31	0.04	0.27	0.03	0.34	0.04
Total	99.09		99.15		99.33		99.55		98.70	

Run No.	KK5-2		KK6-1		KK6-3		KK7-1		KK7-2	
n	25	σ	30	σ	36	σ	28	σ	22	σ
O	0.60	0.36	1.62	0.47	1.46	0.30	1.56	0.48	0.76	0.17
S	36.09	0.37	35.69	0.49	35.93	0.38	36.38	0.52	36.77	0.27
Fe	55.52	0.38	58.06	0.42	57.81	0.35	59.54	0.38	59.99	0.27
Ni	6.62	0.09	3.33	0.06	3.30	0.06	1.60	0.04	1.66	0.06
Cu	0.33	0.04	0.30	0.03	0.30	0.05	0.26	0.02	0.29	0.03
Total	98.83		98.70		98.50		99.07		99.18	

Run No.	KK8-1		KK8-2		KK12-1		KK15-1		KK15-2	
n	25	σ	32	σ	12	σ	33	σ	10	σ
O	0.46	0.11	0.34	0.25	9.22	0.26	6.72	1.09	6.33	0.80
S	37.21	0.22	37.16	0.39	23.74	0.32	30.62	1.21	29.06	0.84
Fe	49.27	0.38	50.27	0.28	65.98	0.39	63.77	0.98	63.99	0.60
Ni	11.54	0.14	11.76	0.20	0.21	0.02	0.29	0.04	0.31	0.02
Cu	0.32	0.07	0.37	0.04	0.24	0.05	0.21	0.02	0.27	0.02
Total	98.49		99.53		99.14		101.40		99.69	

Run No.	KK15-4		KK15-5		KK16-1		KK16-2	
n	13	σ	14	σ	37	σ	36	σ
O	7.06	0.78	7.14	0.61	0.74	0.19	0.75	0.17
S	29.71	0.58	29.07	0.82	36.35	0.27	36.47	0.27
Fe	64.15	0.58	64.92	0.73	62.32	0.37	61.67	0.32
Ni	0.31	0.02	0.32	0.02	0.19	0.02	0.20	0.02
Cu	0.23	0.04	0.30	0.03	0.26	0.02	0.30	0.03
Total	101.23		101.46		99.61		99.09	

Values in wt%. *n* refers to number of analyses.

Figs. 2 and 3 are plots of $D_{\mathrm{M}}^{sulph/sil}$ vs. log[wt% FeO] for the elements investigated here (Table 4). In several experiments the sulphide contained significant amounts of Ni (up to 11.8 wt%), which necessitates small corrections to the data points. The corrections were done by noting that Eq. (8) contains the ratio of FeS activity to FeO activity. Then, assuming that the FeS–NiS solid solution is in Raoult's law region for FeS, the "apparent" corrected FeO content of the silicate melt to be used on Figs. 2 and 3 was obtained from:

$$[\mathrm{FeO}]_{corrected} = \frac{[\mathrm{FeO}]_{silicate}}{[\mathrm{Fe}/(\mathrm{Fe}+\mathrm{Ni})]_{sulph}}$$

where $[\mathrm{Fe}/(\mathrm{Fe}+\mathrm{Ni})]_{sulph}$ is the molar ratio of iron to iron plus nickel in the sulphide. This correction was applied to those data from experiments in which the sulphide contained >0.5 wt% Ni, but was not necessary for the other 11 experiments with Ni contents of the sulphide <0.5%. As can be seen, there are, for many elements, excellent correlations between partition coefficients and the iron contents of the silicate melts. This means, in principle, that the composition of the silicate melt may be used to calculate the sulphide–silicate melt partition coefficient for a wide range of geological scenarios. We discuss some of these in more detail below.

We fitted Eq. (10) to our data on an element by element basis using the linear regression model of the SPSS statistical package. This generated the fitted lines shown in Figs. 2 and 3 and fit parameters given in Table 5. We now discuss the nature of the fit for different elements.

3.3. Pb, Co, Cd

Pb, Co and Cd are divalent elements in virtually all geological environments, dissolving as MO in the silicate and MS in the sulphide. Given that the sulphide is dominantly (Fe, Ni)S we would anticipate a value of $n/2$ close to 1.0. As can be seen from Fig. 2a, c, d and Table 5, these three elements obey the expected relationship fairly closely and the regressed value of $n/2$ is within 2σ of the expected value.

If we fix the slope at -1.0 for these elements then, as shown in Table 5, we reproduce $D_{\mathrm{M}}^{sulph/sil}$ with a standard error of 0.046–0.064, corresponding to an uncertainty of 11–16% in D.

Thermodynamic data on the exchange reaction may be used to estimate the temperature dependence of partition coefficients provided the stoichiometry is well constrained. In this case we can extrapolate our 1673 K data for Pb using the thermodynamic data of Barin et al. (1989) to decompose the regression constant into temperature-dependent (corresponding to enthalpy change) and temperature-independent (corresponding to entropy change) terms as follows:

$$\log D_{\mathrm{Pb}}^{sulph/sil} = -\log \%\mathrm{FeO} + \frac{1755}{T} + 1.51 \quad \left(R^2 = 0.95\right)$$

Thermodynamic data for Cd and Co are incomplete, so this extrapolation is currently restricted to Pb.

3.4. Zn, Mn

Zn is an example of an element for which we find an excellent correlation between $\log D$ and log[wt% FeO] (Fig. 3d), but with a

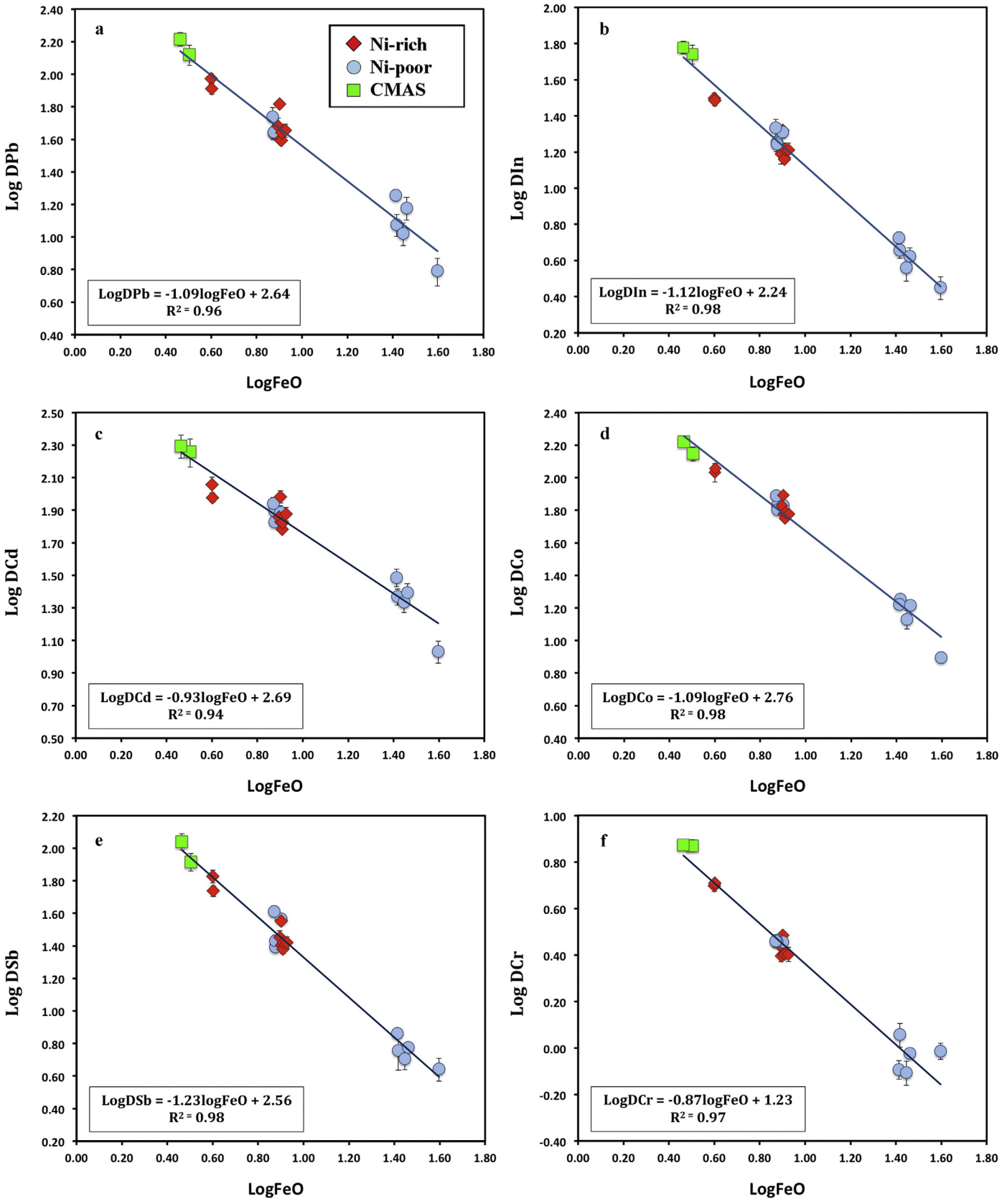

Fig. 2. Log $D^{sulphide/silicate}$ values plotted vs. log FeO content (wt%) of the silicate glass. Partitioning data from Table 4. Error bars (shown where larger than symbols) were calculated from the standard deviations given in Supplementary Tables 1 and 2. Ni-rich (1.6–11.8 wt% Ni in sulphide) and low-Ni experiments performed using a MORB composition (see Table 1). Two experiments (KK16-1, KK16-2) were performed with a CMAS silicate composition and contained 0.5% added NiS. All data were incorporated into the fit. The equation parameters and uncertainties are presented in Table 5.

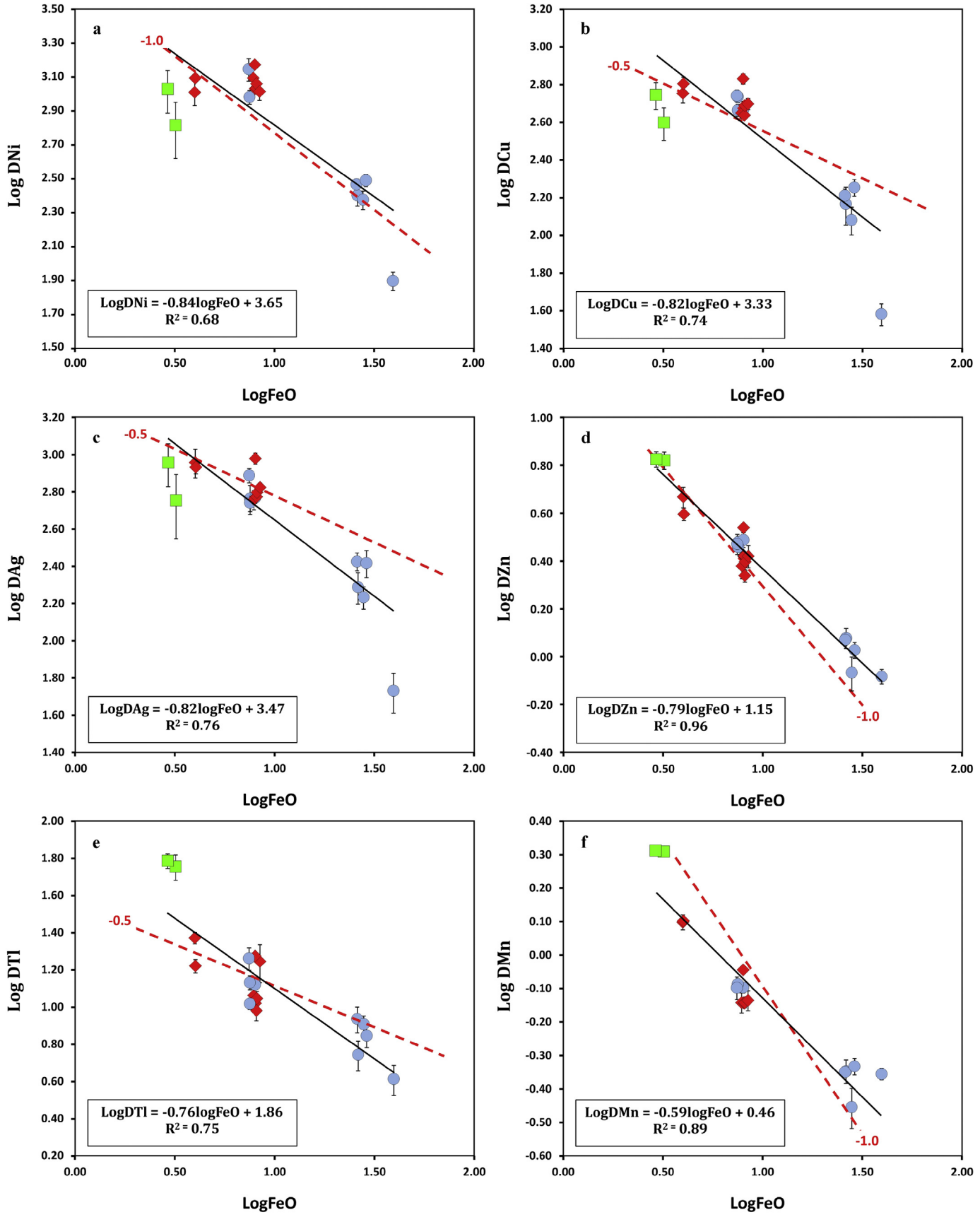

Fig. 3. Log $D^{sulphide/silicate}$ values plotted vs. log FeO content (wt%) of the silicate glass. Legend as in Fig. 2. Partitioning data from Table 4. Error bars (shown where larger than symbols) calculated as in Fig. 2. All data were incorporated into the fit. The equation parameters and uncertainties are given in Table 5. Dotted red lines represent the theoretical slope expected from the valency of the element. Number next to the dotted line characterizes the value for the theoretical slope. (For interpretation of the references to color in this figure legend, the reader is referred to the web version of this article.)

Table 4
Partition coefficients between the sulphide and silicate liquids.

Run No.	KK3-1	σ	KK3-2	σ	KK4-1	σ	KK4-3	σ	KK5-1	σ
Cu	542.8	36.5	461.0	17.7	460.6	33.1	549.6	40.6	471.8	39.6
Ag	581.2	100.8	588.6	39.0	552.5	56.3	775.3	67.9	592.7	38.4
Sb	24.7	1.3	36.8	2.7	27.1	2.1	40.9	3.2	25.3	1.0
Mn	0.8	0.0	0.8	0.0	0.8	0.0	0.8	0.1	0.7	0.0
Co	67.5	1.0	67.8	3.4	63.4	1.0	77.4	2.9	59.9	1.5
Zn	3.0	0.1	3.1	0.2	2.9	0.1	3.0	0.3	2.7	0.1
Cd	78.5	4.9	77.1	7.6	67.2	3.0	87.3	7.8	67.4	1.9
In	17.9	0.5	20.4	1.5	17.6	1.7	21.6	2.4	15.3	0.9
Tl	10.4	0.3	13.2	1.2	13.5	1.2	18.3	2.5	10.5	0.8
Pb	43.8	1.6	45.3	3.8	44.0	4.3	54.7	7.6	39.6	1.8
Cr	2.9	0.1	2.9	0.2	2.9	0.1	2.9	0.2	2.7	0.1
Ni	–	–	–	–	952.4	89.7	1394.0	213.1	1068.2	39.5

Run No.	KK5-2	σ	KK6-1	σ	KK6-3	σ	KK7-1	σ	KK7-2	σ
Cu	445.3	26.4	433.0	15.2	487.3	16.4	496.9	33.4	675.1	41.1
Ag	574.8	68.7	593.9	29.8	627.1	41.3	668.3	38.4	954.9	66.3
Sb	28.3	2.7	24.0	1.5	26.4	1.5	26.4	2.1	35.7	1.6
Mn	0.7	0.0	0.7	0.0	0.7	0.0	0.7	0.0	0.9	0.0
Co	67.1	3.1	56.0	1.4	61.3	1.5	59.9	2.1	78.2	2.2
Zn	2.4	0.3	2.2	0.1	2.5	0.2	2.7	0.3	3.5	0.1
Cd	72.1	6.5	60.6	2.9	66.4	7.4	75.2	7.1	96.0	8.2
In	15.4	1.8	14.4	0.6	16.4	1.4	16.3	1.5	20.9	1.0
Tl	11.5	1.3	9.6	1.2	11.1	1.0	17.6	4.0	18.8	0.9
Pb	47.8	5.9	39.1	1.5	43.9	3.8	45.2	4.1	65.8	3.6
Cr	2.5	0.1	2.5	0.1	2.5	0.1	2.5	0.2	3.0	0.1
Ni	1232.7	164.6	1077.0	28.5	1141.0	12.2	1026.1	117.6	1479.6	68.9

Run No.	KK8-1	σ	KK8-2	σ	KK12-1	σ	KK15-1	σ	KK15-2	σ
Cu	565.3	62.7	636.1	52.8	38.2	4.5	146.4	33.1	162.4	13.5
Ag	909.6	160.2	857.3	67.8	53.9	10.9	194.5	37.2	266.9	29.5
Sb	67.1	5.9	54.6	4.1	4.4	0.6	5.7	1.4	7.3	0.3
Mn	1.3	0.1	1.3	0.0	0.4	0.0	0.4	0.0	0.4	0.0
Co	107.8	13.9	113.8	3.4	7.9	0.2	18.0	0.8	16.7	0.6
Zn	4.7	0.5	4.0	0.2	0.8	0.1	1.2	0.1	1.2	0.1
Cd	113.9	12.9	94.7	5.8	10.8	2.2	23.4	2.7	30.6	3.7
In	31.4	2.2	30.6	2.1	2.8	0.4	4.5	0.5	5.3	0.4
Tl	23.5	1.7	16.6	1.4	4.1	0.9	5.5	1.0	8.6	1.4
Pb	93.8	6.9	81.7	6.4	6.2	1.2	11.9	1.8	18.1	1.5
Cr	5.0	0.3	5.1	0.2	1.0	0.1	1.1	0.1	0.8	0.1
Ni	1444.2	169.7	1781.5	63.1	77.8	8.9	249.8	34.4	289.4	21.9

Run No.	KK15-4	σ	KK15-5	σ	KK16-1	σ	KK16-2	σ
Cu	120.5	20.3	179.1	18.0	396.2	95.1	554.5	93.3
Ag	171.5	23.5	261.9	43.6	569.1	215.3	909.0	234.3
Sb	5.1	0.7	6.0	0.5	82.4	10.1	109.8	12.6
Mn	0.4	0.0	0.5	0.0	2.0	0.1	2.1	0.1
Co	13.5	1.8	16.5	0.5	140.6	14.0	166.8	10.7
Zn	0.9	0.1	1.1	0.1	6.7	0.6	6.7	0.5
Cd	21.7	3.0	24.8	3.3	181.4	35.5	197.2	32.2
In	3.6	0.6	4.2	0.5	55.1	6.5	60.1	4.8
Tl	8.1	0.9	7.0	1.0	56.9	8.8	61.1	5.6
Pb	10.5	1.7	15.1	2.4	132.0	19.1	164.7	15.5
Cr	0.8	0.1	1.0	0.0	7.4	0.5	7.5	0.3
Ni	235.0	29.7	306.0	25.2	648.9	237.1	1065.1	299.8

σ – calculated by error propagation. Between 4 and 13 analyses made of each phase (Supplementary Tables 1 and 2).

slope which implies a valency n significantly different from the expected value of +2. Since Zn has no other plausible valency under the conditions of our experiments, the slope of the relationship must reflect the oxidation state conflated with changing activity coefficients of trace Zn in either the silicate (as ZnO) or sulphide (as ZnS) phases. Activity coefficients of species comparable to ZnO in silicate melts such as FeO, NiO, CoO and CrO are quite weak functions of silicate melt composition (O'Neill and Berry, 2006; O'Neill and Eggins, 2002), which means that the deviation of the slope from −1 is unlikely to be due to changes in the FeO content of the silicate melt. A more likely explanation is that the lithophile character of Zn results in increasing partitioning of Zn into the sulphide as its oxygen content increases. Effectively, the activity coefficient of ZnS in the sulphide decreases as its oxygen content increases. We emphasize this by plotting a slope of −1 in Fig. 3d and showing that, at low oxygen contents of the sulphide (low FeO in the silicate melt), $\log D_{Zn}^{sulph/sil}$ is approximately proportional to $-\log$ %FeO. As oxygen content of the sulphide increases, the slope flattens due to decrease in the ZnS activity coefficient in the sulphide.

We may exclude the major effects of oxygen in the sulphide on $D_{Zn}^{sulph/sil}$ by just considering those data at FeO contents of the silicate melt between 2.9 and 8.1%, corresponding to oxygen contents of the sulphide < 1.6 wt%. Fixing the slope at −1, we obtain an R^2 of 0.84 for this composition range. Using the thermodynamic data of Barin et al. (1989) to decompose the constant term into

Table 5
Equation parameters for the partition coefficients between sulphide and silicate liquids.

Element	$c(A)^*$	σ	Slope*	σ	R^2	Std error	$c(B)^{**}$	σ	a^{***}	b^{***}
In	2.243	0.041	−1.118	0.040	0.979	0.057				
Pb	2.644	0.057	−1.085	0.055	0.958	0.079	2.554	0.064	1.505	1755
Co	2.760	0.043	−1.088	0.042	0.975	0.060	2.665	0.046		
Cd	2.687	0.057	−0.928	0.056	0.942	0.080	2.765	0.060		
Cu	3.334	0.123	−0.823	0.120	0.736	0.172	2.985	0.522	0.851	3570
Ag	3.469	0.115	−0.819	0.112	0.759	0.160	3.124	0.521		
Sb	2.559	0.049	−1.229	0.047	0.975	0.068				
Mn	0.456	0.052	−0.585	0.051	0.886	0.073	0.907	0.148	1.595	−1151
Zn	1.150	0.039	−0.785	0.038	0.961	0.055	1.386	0.079	1.262	208
Tl	1.862	0.109	−0.760	0.106	0.752	0.152	1.581	0.515		
Cr	1.231	0.041	−0.869	0.040	0.965	0.058				
Ni	3.654	0.157	−0.842	0.150	0.676	0.215	3.829	0.166	2.368	2445

* $c(A)$ and slope are the regression parameters for the linear equation $\log D(\text{element}) = \text{slope} \cdot \log \text{FeO} + c$.
** $c(B)$ is the regression constant when the slope of the regression line is fixed at −1 for divalent and −0.5 for monovalent cations.
*** Parameters a and b are used in the equation ($\log D(\text{element}) = \text{slope} \cdot \log \text{FeO} + b/T + a$) for the temperature correction. The slope is fixed at −1 for divalent cations and −0.5 for monovalent.

temperature-dependent and temperature-independent terms leads to:

$$\log D_{\text{Zn}}^{sulph/sil} = -\log \%\text{FeO} + \frac{208}{T} + 1.26$$
$$\left(\text{FeO} \leqslant 8.1 \text{ wt\%};\ R^2 = 0.84\right)$$

Manganese (Fig. 3f) shows similar behavior to Zn, but with an even larger difference between observed and anticipated slope. Values of $\log D_{\text{Mn}}^{sulph/sil}$ are close to 0, however, indicating that Mn is lithophile rather than chalcophile. Hence the increasing compatibility of Mn in the sulphide with increasing oxygen content is even more marked than in the case of Zn. We show below that Mn sulphide–silicate partitioning data from the literature are consistent with this interpretation of increasing partitioning into sulphide with increasing O content. We represent the effect by fitting the data at low concentration of FeO (up to 8.1%) to a slope of −1. With the temperature dependence constrained using the thermodynamic data as before, this yields:

$$\log D_{\text{Mn}}^{sulph/sil} = -\log \%\text{FeO} - \frac{1151}{T} + 1.60$$
$$\left(\text{FeO} \leqslant 8.1 \text{ wt\%};\ R^2 = 0.94\right)$$

3.5. Sb, In

The partition coefficients of antimony and indium both correlate almost perfectly with the FeO contents of the silicate liquid (Fig. 2b, e). In the oxygen fugacity range of our experiments and in high temperature natural environments we expect that both these elements would be in the +3 oxidation state, giving an expected $n/2$ of −1.5. In practice both show slightly lower slopes, suggesting either that they interact with oxygen in the sulphide at high FeO concentrations, that their activity coefficients in the silicates change with FeO content or that they enter the sulphide in mixed oxidation states, for example as +3 and +1. The latter explanation is possible for In, for which the +1 oxidation state is at least known, if not stable, but very unlikely for Sb. We therefore consider it likely that the slope reflects systematic change in activity coefficient with composition, either in the silicate or the sulphide phase.

3.6. Cr

Although we conventionally think of Cr as having the two principal oxidation states of +6 and +3, the divalent oxidation state becomes important in silicate melts at oxygen fugacities below the Ni–NiO buffer (Berry et al., 2006). At 2–3 log f_{O_2} units below NNO, therefore, we anticipate that Cr will be present in the melt as both Cr^{2+} and Cr^{3+} with the former dominant (Berry et al., 2006). Given this, we might expect a slope of $\log D_{\text{Cr}}^{sulph/sil}$ vs. log %FeO of between −1 and −1.5. The observed value of −0.87 ($R^2 = 0.97$) probably indicates a mixture of the effects already discussed.

3.7. Cu, Ag, Tl

These three elements are all present in the +1 oxidation state under the relatively reducing conditions (FMQ-1 log unit) of our experiments. The same oxidation state applies during melting in the mantle and fractional crystallization of basaltic melts (∼ FMQ). As can be seen in Fig. 3b, c, Cu and Ag have very similar sulphide–silicate partition coefficients and similar forms to the graph of $\log D_{\text{M}}^{sulph/sil}$ vs. log %FeO. In neither case does the slope approximate the anticipated value (−0.5) and the apparent relationship is markedly nonlinear. The nonlinear relationship between $\log D_{\text{M}}^{sulph/sil}$ and log %FeO is, we believe, due principally to the opposite effect from that observed in the Mn partitioning data. That is, Cu and Ag are both strongly chalcophile and as the oxygen content of the sulphide increases these two elements are progressively excluded, so the sulphide–silicate partition coefficient is reduced. Other experimental data from the literature, discussed below, support this conclusion. For Cu we can take the data at low FeO contents of the silicate melt, force a slope of −0.5 and obtain, using the thermodynamic data for the Cu–Fe exchange reaction (Barin et al., 1989).

$$\log D_{\text{Cu}}^{sulph/sil} = -0.5 \log \%\text{FeO} + \frac{3570}{T} + 0.85 \qquad (11)$$

Tl, which forms a 1+ ion with strong chemical similarities to K^+ (Goldschmidt, 1954) shows a good correlation between $\log D_{\text{Tl}}^{sulph/sil}$ and log %FeO with the basaltic melts approximating a slope of −0.5 (Fig. 3e). Partitioning involving our CMAS liquid is, however, displaced from an extrapolation of the principal line due, we believe, to the large differences in silicate melt composition. A recent study of Tl partitioning between Fe-rich metal and silicate melt (Wood et al., 2008) demonstrated a large, as yet uncalibrated, effect of silicate composition on the metal–silicate Tl partition coefficient. Our data show a similar effect.

3.8. Ni

Our data for Ni are subject to considerable uncertainty because of the large proportions of Ni lost from capsules during the experiments. Nevertheless, the general trend of the Ni data (Fig. 3a)

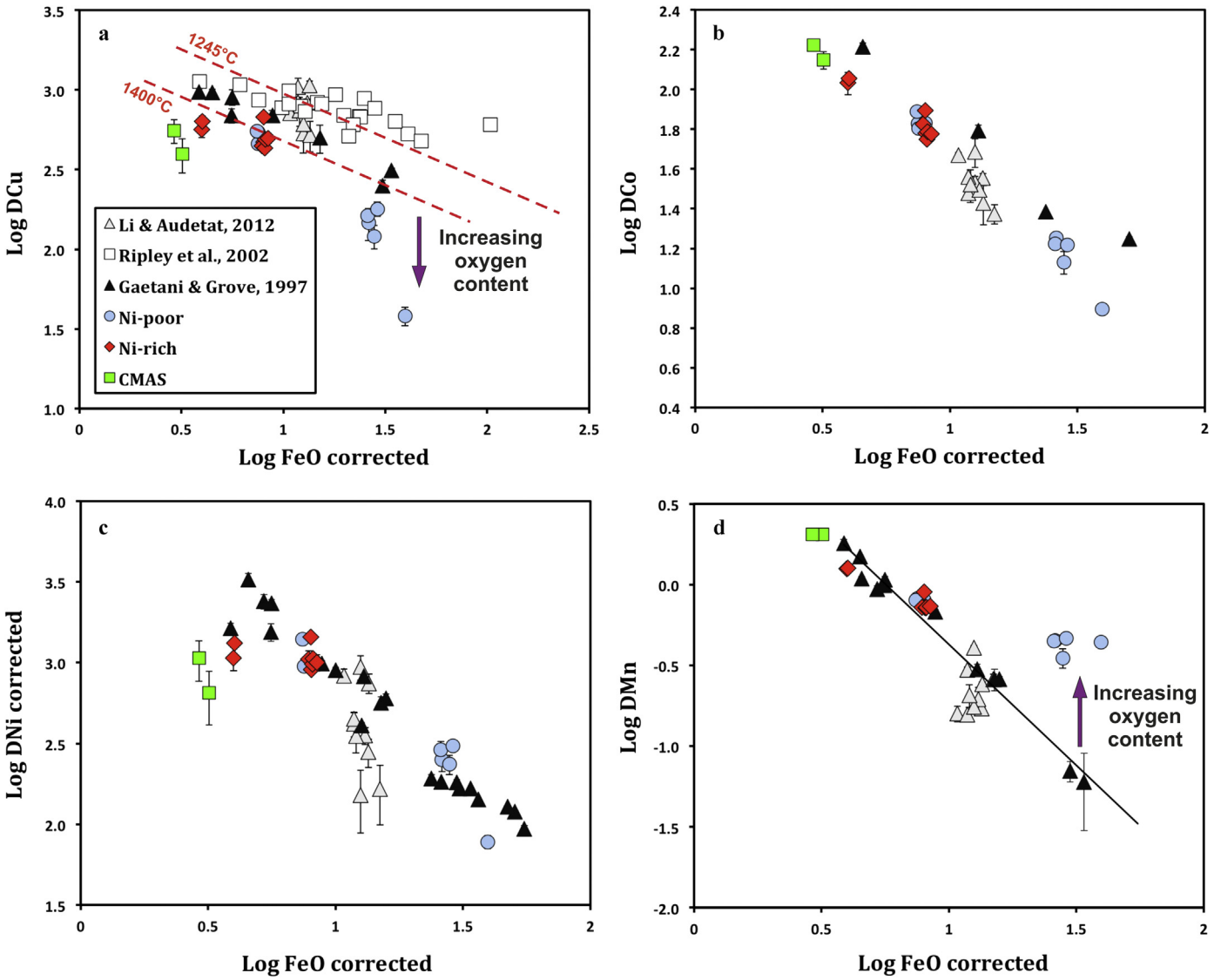

Fig. 4. Comparison of Cu, Ni, Mn and Co partition coefficients obtained in this study with other data in the literature. Given that sulphide compositions frequently have elevated Ni and Cu contents, we correct the X axis by dividing wt% FeO in the silicate melt by molar [Fe/(Fe + Ni + Cu)] in the sulphide (see text). Lines denoted 1245 °C and 1400 °C illustrate the shift in D_{Cu} predicted from Eq. (11). Data of Ripley et al. (2002) are at 1245 °C, Gaetani and Grove (1997) at 1350 °C and Li and Audétat (2012) at 1175–1300 °C. Our results refer to 1400 °C.

is consistent with that for the other 2+ elements so we consider that our results are indicative of Ni behavior if not as definitive as those for most of the other elements. In Fig. 3a we have corrected the Ni partitioning data for Fe content of the sulphide as discussed above and have added a correction for the fact that Ni is a major element in the sulphide liquid in some experiments. In the latter cases we need to correct for the differences in activity coefficient of NiS between a Ni-rich sulphide and pure FeS. We performed this correction using data on FeS–NiS melts (Fleet, 1989), which we have simplified to treat as a regular solution with activity coefficient for NiS given by:

$$\log \gamma_{NiS} = 0.94\left[\frac{Fe}{Fe+Ni}\right]^2_{sulph}$$

The correction then involves subtracting the activity term for pure FeS from $\log D_{Ni}^{sulph/sil}$ and adding the equivalent term for the Fe/Ni ratio of the sulphide in the experiment. The shifts are small for our experiments, a maximum displacement of −0.15 in $\log D_{Ni}^{sulph/sil}$.

3.9. Comparison with previous studies

Having developed a thermodynamically-based model which describes sulphide–silicate partitioning for a wide range of elements, it is appropriate now to consider how well our model reproduces results from other studies. Fig. 4 shows comparisons between our data and those of Ripley et al. (2002), Li and Audétat (2012) and Gaetani and Grove (1997).

Li and Audétat (2012) reported partitioning of V, Mn, Co, Ni, Cu, Zn, As, Mo, Ag, Sn, Sb, W, Au, Pb and Bi between monosulphide solid solution, sulphide liquid and hydrous silicate melt at the range of temperatures (1175–1300 °C), pressures (1–3 GPa) and oxygen fugacities (QFM-3.1 to QFM+1). Although their results cover a narrow range of FeO contents (Fig. 4a–d), it can be seen that there is very good agreement between their data and ours for the elements Co, Cu, Ni and Mn. The data of Li and Audétat (2012) for Pb and Ag also agree well with our results but there is a small offset of about −0.5 log units in $\log D$ for Sb and Zn. Although we are unsure of the reason for the small discrepancy, we note that our data for Sb

and Zn both follow the prediction of Eq. (10) extremely closely (Figs. 2e, 3d).

Gaetani and Grove (1997) determined sulphide–silicate partitioning of V, Cr Mn, Co, Ni and Cu, at 1 atm pressure, 1350 °C and under a range of oxygen and sulphur fugacities (between −7.9 and −10.3 log units f_{O_2} and −1.5 to −2.5 log units f_{S_2}). When plotted as a function of the corrected FeO content of the silicate liquid (Fig. 4a–d), their data for Cu, Co, Ni and Mn all show the linear relationship between $\log D$ and $\log$[wt% FeO] predicted from Eq. (10). All of the sulphide liquids produced by these authors contain substantial amounts of Ni, however (7.9–56.8 wt%), which necessitated correction of the apparent FeO contents of the silicate liquids in the manner discussed above. Despite the large FeO-corrections to some results, agreement of our data on FeS-rich sulphides with those on Ni-rich sulphides indicates that our model has wide applicability. Individually, when we consider the results of Gaetani and Grove (1997) on Cu and Mn, we observe the effects of increasing O content of the sulphide liquid on partitioning discussed earlier in this section. The two lowest partition coefficients for Mn and Cu measured by Gaetani and Grove refer to sulphides in which Fe/(Fe + Ni + Cu) was 0.3 and 0.4. Hence the data have been shifted to the right on the log[%FeO] axis by 0.5 and 0.4 log units respectively. The oxygen contents of these sulphide liquids, which were not measured by Gaetani and Grove, should be about 2% (Fig. 1b), whereas the corresponding oxygen contents for our FeS-rich experiments with which we are comparing their data are 7–9%. We therefore conclude, as indicated in Fig. 4, that increasing O content of the sulphide tends to partition lithophile Mn more strongly and chalcophile Cu less strongly into this phase.

Ripley et al. (2002) measured Cu partitioning between Cu-rich (9–74% Cu) sulphides and silicate melts at 1245 °C and 1 atm pressure. In this case we correct the FeO content of the silicate liquid by taking account of the Cu content of the sulphide in the manner described above:

$$[\mathrm{FeO}]_{corrected} = \frac{[\mathrm{FeO}]_{silicate}}{[\mathrm{Fe}/(\mathrm{Fe}+\mathrm{Ni}+\mathrm{Cu})]_{sulphide}} \quad (12)$$

The data give slightly higher partition coefficients than ours and those of Gaetani and Grove (1997), but maintain the correct dependence on FeO content of the silicate melt (Fig. 4a). When the effects of temperature are accounted for using Eq. (11) we predict that the Ripley et al. (2002) data should have $\log D_{Cu}$ about 0.22 log units higher at 1245 °C than our results at 1400 °C. As can be seen from Fig. 4a, this displacement is in agreement with that observed. We do not, however, find such good agreement with the results of Holzheid and Lodders (2001), who used essentially pure Cu_2S melts in their study of Cu solubility at 1 atm pressure.

4. Discussion

We turn now to considering some of the geological applications of our new data and the straightforward relationships between $\log D_M^{sulph/sil}$ and $\log$%FeO.

4.1. Ce/Pb and Nd/Pb in MORB

Ce, Nd and Pb are all relatively incompatible in silicates, but Ce and Nd have moderate partition coefficients into clinopyroxene (Wood and Blundy, 1997), while Pb partition coefficients into clinopyroxene are generally around 0.1 (Hart and Dunn, 1993; Klemme et al., 2002). In order to maintain the approximately constant Ce/Pb and Nd/Pb ratios found in MORB, the partitioning of Pb into residual sulphide has been proposed as a counterbalance to the higher partition coefficients of Ce and Nd into residual clinopyroxene. We modeled these effects by calculating the Ce, Nd and Pb concentrations expected from partial melting of depleted (MORB) mantle and comparing them with a recently-published (Jenner and O'Neill, 2012) database of ocean-floor basaltic glass compositions. We then calculated fractionation paths to compare the results with relatively differentiated compositions.

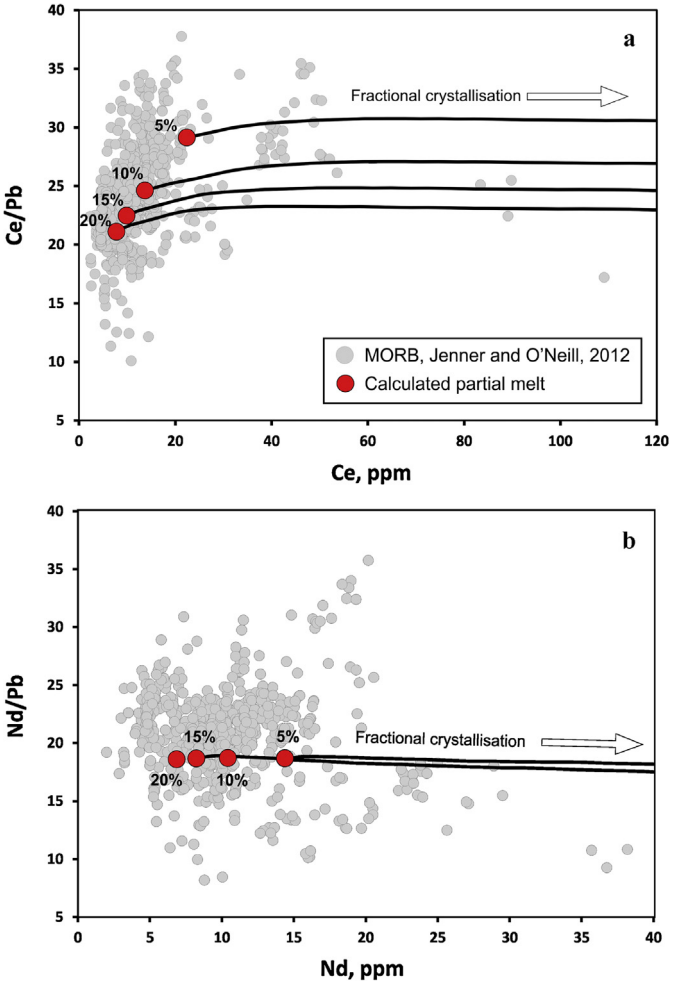

Fig. 5. Calculated Ce/Pb and Nd/Pb ratios for batch partial melts (non-modal) of depleted mantle containing 65 ppb Pb, 1475 ppb Ce and 1130 ppb Nd and their differentiates (see text). Clinopyroxene-melt partition coefficients: Ce = 0.12; Nd = 0.25 (Wood and Blundy, 1997); Pb = 0.1 (Hart and Dunn, 1993; Klemme et al., 2002). $D_{Pb}^{sulph/sil} = 44$ at 8.15% FeO in the melt (this study). Other D values in Supplementary Table 3.

Fig. 5 shows the results of calculated partial melts of depleted mantle assuming non-modal batch melting and a mantle melting reaction obtained at 1.5 GPa (Robinson et al., 1998):

$$0.83\ \text{clinopyroxene} + 0.33\ \text{orthopyroxene} + 0.08\ \text{spinel} = 1\ \text{liquid} + 0.24\ \text{olivine}$$

Clinopyroxene-melt partition coefficients were taken to be 0.12 and 0.25 for Ce and Nd respectively (from Wood and Blundy, 1997) and 0.1 for Pb (Supplementary Table 3). The sulphide–silicate partition coefficient for Pb is calculated to be 44 from Table 5 if we assume a primitive MORB FeO content of 8.15% (Falloon and Green, 1987). The sulphur content of sulphide-saturated MORB was taken from Mavrogenes and O'Neill (1999), while the mass fraction of sulphide in the initial mantle is given by its S content in ppm divided by the S content of sulphide, 3.6×10^5. Ce and Nd were assumed not to partition into sulphide. Additional silicate-melt partition coefficients are given in Supplementary Table 3.

If we start with the depleted mantle composition of Salters and Stracke (2004), containing 119 ppm S, 772 ppb Ce, 713 ppb Nd

and 23.2 ppb Pb, our partial melts and fractional crystallization products have high values of Ce/Pb ~ 30, with Nd/Pb ~ 28 and Pb contents well below those of the most primitive MORB measured by Jenner and O'Neill (2012). If, on the other hand, we start with the primitive mantle composition of McDonough and Sun (1995) (250 ppm S, 1675 ppb Ce, 1250 ppb Nd, 150 ppb Pb) we obtain low Ce/Pb of ~ 12 and Nd/Pb of ~ 9. Therefore we require a Pb content of the depleted mantle which is intermediate between these initial two estimates. We proceeded by noting that the continental crust is approximately 0.6% of the mass of the silicate Earth and that it has estimated Ce, Nd and Pb contents of 42, 20 and 12.6 ppm (Rudnick, 1995). If we assume that continental crust is the principal complement to the depleted mantle then, assuming that depleted mantle plus continental crust sums to bulk silicate Earth, the depleted mantle should contain ~ 1425 ppb Ce (1675 ppb in primitive mantle) ~ 1130 ppb Nd (1250 ppb in primitive mantle) and ~ 74 ppb Pb (150 ppb). For Ce and Nd the differences between primitive and depleted mantles are small, so it is the concentration of Pb, which has most leverage on the result. Starting with an assumed mantle S content of 250 ppm we adjusted the initial Pb content of depleted mantle to 65 ppb in order to obtain the fit shown in Fig. 5. As can be seen, the predicted Nd/Pb ratio of the melt is insensitive to the extent of melting and the degree of fractionation over a wide range of Nd concentrations or extents of fractionation, a relationship already noted from the compositions of oceanic basalts (Hofmann, 2003). This close agreement with observation gives us some confidence in the adopted value of Pb content of the depleted mantle, provided our estimate of S content is approximately correct. In the case of Ce/Pb, there is a slight dependence of ratio on degree of melting, but a result close to the canonical value of 25 is readily obtained. If we reduce the S content of depleted mantle from 250 to 150 ppm then we only reduce the "best-fit" value of Pb in the depleted mantle from 65 to 55 ppb, while raising S to 350 ppm would move Pb in the mantle to 70 ppb. The result appears relatively robust. Fractionation calculations were performed assuming Rayleigh fractionation and the MORB assumed to crystallize olivine alone for the first 10% of fractionation, followed by an olivine–clinopyroxene mixture in ratio 3:7 together with the small amount of sulphide required to precipitate in order to remain at sulphide saturation. As can be seen and as expected, neither Nd/Pb nor Ce/Pb should change greatly during > 50% of fractional crystallization.

4.2. Chalcophile elements in the depleted mantle

Having applied the data of Jenner and O'Neill (2012) on basaltic glasses to the question of Ce/Pb and Nd/Pb in mantle-derived melts, we may use the same data to estimate the concentrations of other chalcophile elements in the depleted mantle sources of MORB. Primitive MORB glasses in their study contain ~ 100 ppm Cu, ~ 30 ppb Ag, 60 ppb In, 100 ppb Cd and have Pb/Sb and Pb/Tl ratios of 40 and 49 respectively. Using the sulphide–silicate partition coefficients of this study (other data in Supplementary Table 3) and assuming 8.15% FeO in a 10% batch melt with 250 ppm S in the mantle, leads to the following concentrations in the depleted mantle: 32 ppm Cu, 7.6 ppb Ag, 12 ppb In, 23 ppb Cd, 1.7 ppb Sb and 1.3 ppb Tl. The values for Cu, Ag and In are in very good agreement with the estimates of Salters and Stracke (2004), while those for Cd and Tl are higher and that for Sb lower than these authors estimated. If we reduce the S content of the depleted mantle to 150 ppm, however, the In, Cd, Tl and Sb values change little, but those for Cu and Ag are reduced to about 60% of the previous estimates. This is because the latter two elements partition much more strongly into sulphide than do In, Cd, Tl and Sb (Table 5).

5. Conclusions

Although trace element partitioning between sulphide liquids and silicate melts depends on the ratio of the fugacity of sulphur to that of oxygen, we have shown that partition coefficients may be re-formulated to eliminate this ratio and replace it with $\frac{a_{FeS}^{sulph}}{a_{FeO}^{sil}}$. The latter ratio may in principle be calculated from the compositions of sulphide and silicate phases because the activity coefficients of FeO in silicate melts are close to 1 (O'Neill and Eggins, 2002) and the sulphide is close to pure FeS, which means that its activity coefficient and activity are also close to 1. Applying these approximations, we showed that trace element partitioning between FeS liquid and silicate melt should generally exhibit a linear relationship between $\log D_M^{sulph/sil}$ and the logarithm of the FeO content of the silicate melt with a slope which depends on the valency of the trace metal. Most elements studied behave as expected, although the slope of the relationship between partitioning and FeO content may deviate from the expected one because of nonideal solution in the sulphide or silicate phases.

Given the framework provided by this study and the simple relationships observed between $\log D_M^{sulph/sil}$ and log %FeO, we consider that extension of the data in temperature and composition space should be relatively straightforward. For a number of the elements of interest thermodynamic data should enable temperature extrapolation to be made. Testing of such extrapolations are experimentally feasible using graphite capsules such as those we have employed. Since sulphide precipitation is an important feature of oceanic basalts and arc and continental volcanics, there is a need for data on more SiO_2-rich compositions than those used in this study and for the effects of large amounts of dissolved water to be clarified. We are currently engaged in extending the scope of this research to address these questions.

Acknowledgements

We acknowledge helpful discussions with our colleagues Andrew Matzen, Ashley Norris, James Tuff and Jon Wade. We thank Tim Elliott, James Brenan and an anonymous reviewer for their valuable comments. This research was supported by European Research Council grant 267764.

Appendix A. Supplementary material

Supplementary material related to this article can be found online at http://dx.doi.org/10.1016/j.epsl.2013.09.034.

References

Barin, I., Sauert, F., Schultze-Rhonhof, E., Sheng, W.S., 1989. Thermochemical Data of Pure Substances, Part I and Part II. CH Verlagsgesellschaft, Weinheim, Germany.

Berry, A.J., O'Neill, H.S., Scott, D.R., Foran, G.J., Shelley, J.M.G., 2006. The effect of composition on Cr^{2+}/Cr^{3+} in silicate melts. Am. Mineral. 91, 1901–1908.

Bockrath, C., Ballhaus, C., Holzheid, A., 2004. Fractionation of the platinum-group elements during mantle melting. Science 305, 1951–1953.

Burton, K.W., Cenki-Tok, B., Mokadem, F., Harvey, J., Gannoun, A., Alard, O., Parkinson, I.J., 2012. Unradiogenic lead in Earth's upper mantle. Nat. Geosci. 5, 570–573.

Crocket, J.H., Fleet, M.E., Stone, W.E., 1997. Implications of composition for experimental partitioning of platinum-group elements and gold between sulfide liquid and basalt melt: The significance of nickel content. Geochim. Cosmochim. Acta 61, 4139–4149.

Dreibus, G., Palme, H., 1996. Cosmochemical constraints on the sulfur content in the Earth's core. Geochim. Cosmochim. Acta 60, 1125–1130.

Falloon, T.J., Green, D.H., 1987. Anhydrous partial melting of MORB pyrolite and other peridotite compositions at 10 kbar – implications for the origin of primitive MORB glasses. Mineral. Petrol. 37, 181–219.

Fellows, S.A., Canil, D., 2012. Experimental study of the partitioning of Cu during partial melting of Earth's mantle. Earth Planet. Sci. Lett. 337–338, 133–143.
Fleet, M.E., 1989. Activity coefficients for FeS and NiS in monosulfide liquid and $NiSi_{1/2}O_2$ in olivine from sulfide–silicate equilibria. Geochim. Cosmochim. Acta 53, 791–796.
Fleet, M.E., Crocket, J.H., Stone, W.E., 1996. Partitioning of platinum-group elements (Os, Ir, Ru, Pt, Pd) and gold between sulfide liquid and basalt melt. Geochim. Cosmochim. Acta 60, 2397–2412.
Fleet, M.E., Stone, W.E., Crocket, J.H., 1991. Partitioning of palladium, iridium, and platinum between sulfide liquid and basalt melt-effects of melt composition, concentration, and oxygen fugacity. Geochim. Cosmochim. Acta 55, 2545–2554.
Fonseca, R.O.C., Campbell, I.H., O'Neill, H.S.C., Fitzgerald, J.D., 2008. Oxygen solubility and speciation in sulphide-rich mattes. Geochim. Cosmochim. Acta 72 (11), 2619–2635, http://dx.doi.org/10.1016/J.Gca.2008.03.009.
Gaetani, G.A., Grove, T.L., 1997. Partitioning of moderately siderophile elements among olivine, silicate melt, and sulfide melt: Constraints on core formation in the Earth and Mars. Geochim. Cosmochim. Acta 61, 1829–1846.
Goldschmidt, V.M., 1954. Geochemistry. Clarendon Press, Oxford.
Hart, S.R., Dunn, T., 1993. Experimental cpx/melt partitioning of 24 trace-elements. Contrib. Mineral. Petrol. 113, 1–8.
Hart, S.R., Gaetani, G.A., 2006. Mantle Pb paradoxes: the sulfide solution. Contrib. Mineral. Petrol. 152, 295–308.
Hofmann, A.W., 2003. Sampling mantle heterogeneity through Oceanic Basalts: isotopes and trace elements. In: Holland, H.D., Turekian, K.K. (Eds.), Treatise on Geochemistry, pp. 61–101.
Hofmann, A.W., Jochum, K.P., Seufert, M., White, W.M., 1986. Nb and Pb in oceanic basalts – new constraints on mantle evolution. Earth Planet. Sci. Lett. 79, 33–45.
Holzheid, A., Grove, T.L., 2002. Sulfur saturation limits in silicate melts and their implications for core formation scenarios for terrestrial planets. Am. Mineral. 87, 227–237.
Holzheid, A., Lodders, K., 2001. Solubility of copper in silicate melts as function of oxygen and sulfur fugacities, temperature, and silicate composition. Geochim. Cosmochim. Acta 65, 1933–1951.
Jenner, F.E., O'Neill, H.S., 2012. Analysis of 60 elements in 616 ocean floor basaltic glasses. Geochem. Geophys. Geosyst. 13, Q02005, http://dx.doi.org/10.1029/2011gc004009.
Klemme, S., Blundy, J.D., Wood, B.J., 2002. Experimental constraints on major and trace element partitioning during partial melting of eclogite. Geochim. Cosmochim. Acta 66, 3109–3123.
Lee, C.T.A., Luffi, P., Chin, E.J., Bouchet, R., Dasgupta, R., Morton, D.M., Le Roux, V., Yin, Q.Z., Jin, D., 2012. Copper systematics in arc magmas and implications for crust–mantle differentiation. Science 336, 64–68.
Li, Y., Audétat, A., 2012. Partitioning of V, Mn, Co, Ni, Cu, Zn, As, Mo, Ag, Sn, Sb, W, Au, Pb, and Bi between sulfide phases and hydrous basanite melt at upper mantle conditions. Earth Planet. Sci. Lett. 355–356, 327–340.
Mathez, E.A., 1976. Sulfur solubility and magmatic sulfides in submarine basalt glass. J. Geophys. Res. 81, 4269–4276.
Mavrogenes, J.A., O'Neill, H.S.C., 1999. The relative effects of pressure, temperature and oxygen fugacity on the solubility of sulfide in mafic magmas. Geochim. Cosmochim. Acta 63, 1173–1180.
McDonough, W.F., Sun, S.S., 1995. The composition of the Earth. Chem. Geol. 120, 223–253.
Meijer, A., Kwon, T.-T., Tilton, G.R., 1990. U–Th–Pb partitioning behavior during partial melting in the upper mantle: Implications for the origin of high μ components and the "Pb Paradox". J. Geophys. Res. 95, 433–448.
Nagamori, M., Yazawa, A., 2001. Thermodynamic observations of the molten FeS–FeO system and its vicinity at 1473 K. Metall. Mater. Trans., B Process Metall. Mater. Proc. Sci. 32, 831–837.
O'Neill, H.S.C., 1991. The origin of the Moon and the early history of the Earth – a chemical model. 2. The Earth. Geochim. Cosmochim. Acta 55, 1159–1172.
O'Neill, H.S.C., Berry, A.J., 2006. Activity coefficients at low dilution of CrO, NiO and CoO in melts in the system $CaO–MgO–Al_2O_3–SiO_2$ at 1400 °C: Using the thermodynamic behaviour of transition metal oxides in silicate melts to probe their structure. Chem. Geol. 231, 77–89.
O'Neill, H.S.C., Eggins, S.M., 2002. The effect of melt composition on trace element partitioning: an experimental investigation of the activity coefficients of FeO, NiO, CoO, MoO_2 and MoO_3 in silicate melts. Chem. Geol. 186, 151–181.
Presnall, D.C., Dixon, S.A., Dixon, J.R., Odonnell, T.H., Brenner, N.L., Schrock, R.L., Dycus, D.W., 1978. Liquidus phase relations on join diopside–forsterite–anorthite from 1 am to 20 kbar – their bearing on generation and crystallization of basaltic magma. Contrib. Mineral. Petrol. 66, 203–220.
Ripley, E.M., Brophy, J.G., Li, C.S., 2002. Copper solubility in a basaltic melt and sulfide liquid/silicate melt partition coefficients of Cu and Fe. Geochim. Cosmochim. Acta 66, 2791–2800.
Robinson, J.A.C., Wood, B.J., Blundy, J.D., 1998. The beginning of melting of fertile and depleted peridotite at 1.5 GPa. Earth Planet. Sci. Lett. 155, 97–111.
Rudge, J.F., Kleine, T., Bourdon, B., 2010. Broad bounds on Earth's accretion and core formation constrained by geochemical models. Nat. Geosci. 3, 439–443.
Rudnick, R.L., 1995. Making continental crust. Nature 378, 571–578.
Salters, V.J.M., Stracke, A., 2004. Composition of the depleted mantle. Geochem. Geophys. Geosyst. 5, Q05B07.
Tuff, J., Wood, B.J., Wade, J., 2011. The effect of Si on metal–silicate partitioning of siderophile elements and implications for the conditions of core formation. Geochim. Cosmochim. Acta 75, 673–690.
Wallace, P., Carmichael, I.S.E., 1992. Sulfur in basaltic magmas. Geochim. Cosmochim. Acta 56, 1863–1874.
Warren, J.M., Shirey, S.B., 2012. Lead and osmium isotopic constraints on the oceanic mantle from single abyssal peridotite sulfides. Earth Planet. Sci. Lett. 359, 279–293.
Wood, B.J., Blundy, J.D., 1997. A predictive model for rare earth element partitioning between clinopyroxene and anhydrous silicate melt. Contrib. Mineral. Petrol. 129, 166–181.
Wood, B.J., Halliday, A.N., 2005. Cooling of the Earth and core formation after the giant impact. Nature 437, 1345–1348.
Wood, B.J., Halliday, A.N., 2010. The lead isotopic age of the Earth can be explained by core formation alone. Nature 465, 767–771.
Wood, B.J., Wade, J., 2013. Activities and volatilities of trace components in silicate melts: a novel use of metal–silicate partitioning data. Contrib. Mineral. Petrol. 166, 911–921.
Wood, B.J., Nielsen, S.G., Rehkamper, M., Halliday, A.N., 2008. The effects of core formation on the Pb- and Tl-isotopic composition of the silicate Earth. Earth Planet. Sci. Lett. 269, 325–335.
Yoshikigravelsins, K.S., Toguri, J.M., 1993. Oxygen and sulfur solubilities in Ni–Fe–S–O melts. Metall. Trans. B 24 (5), 847–856, http://dx.doi.org/10.1007/Bf02663145.